Measurement of Stratus Cloud and Drizzle Parameters in ASTEX with a K_α-Band Doppler Radar and a Microwave Radiometer

A. S. FRISCH, C. W. FAIRALL, AND J. B. SNIDER

NOAA Environmental Technology Laboratory, Boulder, Colorado

(Manuscript received 1 June 1994, in final form 28 September 1994)

ABSTRACT

Data are used from a K_α-band radar and microwave radiometer along with a droplet model to determine the droplet parameters of drizzle and clouds. Drizzle droplet parameters are determined from the zeroth, first, and second moments of the Doppler spectrum. Cloud droplet parameters are determined from the zeroth moment of the Doppler spectrum and the measured integrated liquid water. Measurements of stratus clouds were made during the Atlantic Stratocumulus Transition Experiment (ASTEX) on the island of Porto Santo in the Madeira Islands, Portugal. Potential applications of this technique would be in the long-term monitoring of stratus clouds and in determining the vertical profiles of cloud liquid water, number of cloud droplets, and modal radius.

1. Introduction

Marine stratocumulus and broken clouds are important in boundary layer dynamics and global climate. Marine boundary layer (MBL) clouds strongly influence surface energy transfers because their high albedos (compared with the ocean background) give rise to large deficits in absorbed solar radiative flux at the top of the atmosphere, while their low altitude prevents significant compensations in thermal emission (Randall et al. 1984; Albrecht et al. 1988). Recently, attention has been focused on the physical processes responsible for the presence of broken MBL clouds versus stratocumulus. Investigation of this subject was the goal of the Atlantic Stratocumulus Transition Experiment (ASTEX) held in the North Atlantic in June 1992.

Possible reasons for the transition from stratocumulus to broken clouds include thermodynamic instability such as the cloud-top entrainment instability (Randall 1980; Betts and Ridgway 1989), the diurnal decoupling of the cloud and subcloud layer by solar radiative warming (Betts 1989), and the decoupling effects of drizzle (Albrecht 1989). Drizzle is of interest not only for dynamical reasons but also because it may play a role in interactions between droplet microphysics and cloud condensation nuclei (CCN) (Baker and Charlson 1990), which affect the equilibrium droplet spectra and optical properties. There is also some speculation that large droplets themselves are radiatively important (Wiscombe et al. 1984). Certainly a great deal of effort has been devoted to developing simple one-dimensional MBL models (e.g., Duynkerke and Driedonks 1987; Wang 1992; Bechtold et al. 1992) that can describe both stratocumulus and broken clouds. Only recently have serious efforts been made to incorporate drizzle effects into such models (Albrecht 1992; Wang 1992). So far, this work has been exploratory, using essentially ad hoc drizzle parameterizations. Thus, such models must remain incomplete until an accurate parameterization of drizzle processes is developed. This is a formidable task because the physics requires that such a parameterization include both cloud liquid water content and CCN.

Despite the recognized potential importance of drizzle in regulating MBL thermodynamic structure and MBL-radiative coupling, direct observations of drizzle are relatively rare (see Brost et al. 1982; Nicholls and Leighton 1986). A climatology of drizzle droplet spectra, liquid water content, and moisture fluxes is not available, and many aspects of the basic physical processes of the formation and evaporation of drizzle are not understood. For example, the relative importance of condensation and entrainment effects versus coagulation in the formation of drizzle are controversial (Telford and Wagner 1981; Nicholls 1987). The most detailed examination of drizzle microphysics to date is the classic modeling and measurement case study of Nicholls (1987). For one specification of cloud properties, Nicholls found that drizzle removed moisture from the cloud at a rate of 0.23 g m^{-3} h^{-1} but that this rate decreased by a factor of 10 with a factor of 2 reduction in integrated cloud liquid water content. This prompted Nicholls to suggest that drizzle processes limit the liquid water content of low clouds, an interesting supplement to Albrecht's (1992) comment that

Corresponding author address: Dr. Shelby Frisch, NOAA Environmental Technology Laboratory, Mail Code R/E/ET6, 325 Broadway, Boulder, CO 80303.

from equilibrium thermodynamic considerations drizzle limits the height of low clouds.

Remote sensors such as radar offer an alternative approach to the study of cloud and drizzle properties. However, conventional "weather" radars lack the sensitivity to detect clouds and most drizzle, so the vast majority of radar precipitation studies are devoted to deep convection or at least rain rates greater than 1 mm h^{-1}. In this paper, we report on measurements made with a radar more suited to cloud and drizzle studies: an 8.66-mm wavelength Doppler radar (Kropfli et al. 1990). The short wavelength and sensitivity of this radar permit detection of low-level marine clouds with liquid water contents as low as 0.03 g m^{-3}, and the Doppler feature permits direct determination of drizzle rates as low as 0.01 mm h^{-1}. In addition to the radar, we use a microwave radiometer to give the total integrated cloud liquid water. This is used for estimating the liquid water profiles in nonprecipitating clouds.

The measurements we report on here were obtained on the island of Porto Santo, in the Madeira Islands, Portugal, during the ASTEX field program. There were research aircraft stationed on Santa Maria in the Azores, but unfortunately, there were no flights over Porto Santo during cloud cover, so we have no way to directly compare our results with any in situ observations. The radar was operated in a variety of modes—including vertically pointing—and in several different scanning cycles. For this paper, we restrict our analysis to 25-min periods in which the radar was pointed vertically. The measurements of interest are profiles of radar reflectivity, Doppler velocity, and Doppler spectral width. From these three measurements we determine three basic parameters of a lognormal model of the drizzle spectrum from simple mathematical relationships between the parameters and the moments of the Doppler spectrum implied by the droplet spectrum. These parameters are drop concentration, modal radius, and the distribution width. This allows us to deduce vertical profiles of the drizzle liquid water content, the drizzle flux, and the drizzle-induced moisture and warming time tendencies in the MBL.

In the absence of drizzle, the radar is extremely sensitive to scattering by cloud droplets. Because the mean fall velocity of cloud droplets is negligible (from the measurement point of view) and their Doppler width is dominated by turbulence, unambiguous cloud droplet microphysical information from the radar is limited to the reflectivity. However, by using a typical value for the cloud droplet distribution width, we can obtain the other two distribution parameters from radar reflectivity and microwave radiometer measurements of the integrated cloud liquid water content. This yields an estimate of the mean cloud droplet number concentration plus properties of cloud water density, radius, and related microphysical properties.

In this paper, we demonstrate the application of the millimeter-wavelength (K_α-band) radar for cloud and drizzle measurements by examining two cases from the ASTEX field program. The structure of the paper is as follows: the theoretical development of the Doppler velocity moments and the drizzle and cloud properties are given in sections 2 and 3, the experimental details are given in section 4, the results are presented in section 5, and our conclusions are discussed in section 6.

2. Theory

Relating the radar-measured parameters to properties of drizzle or cloud droplets involves several steps. We begin by specifying a simple model for the droplet size number density that can be applied to both cloud and drizzle droplet modes. We then derive the Doppler velocity spectrum determined through the standard relationships between the scattering cross section and drop fall velocities as a function of their size. For drizzle, we relate the lower moments of the observed Doppler spectrum to the relevant properties of the drizzle. For our purposes it is sufficient to compute the zeroth moment (characterized by the reflectivity factor Z), the first moment (mean fall velocity), and the second moment about the mean (width of the Doppler spectrum). From an atmospheric dynamics point of view, we are most interested in the drizzle moisture flux divergence, which requires diagnosis of the drizzle liquid water content and fall velocity as a function of height. For clouds, the first and second moment contain no usable information about the distribution, so we need additional constraints or measurements (which are discussed below).

a. Droplet spectrum

The droplet number density spectrum $n(r)dr$ defines the number of droplets per unit volume between radius $r - dr/2$ and $r + dr/2$, where dr denotes an infinitesimal radius increment. Rain is typically characterized by an exponential distribution, often referred to as a Marshall–Palmer distribution (Marshall and Palmer 1948) or a Gamma distribution (Ulbrich 1983; Willis 1984). We have chosen to use a lognormal distribution, which has the same number of free parameters as the Gamma distribution but is computationally more convenient (Borovikov 1961; Levin 1961; Atlas et al. 1989; White et al. 1991) and has also been used to characterize cloud droplets (Davidson et al. 1984). Also, most previous work has been done on much larger rainfall rates than the drizzle we are considering, so we have no reason to expect established empirical relationships to be applicable. This spectrum takes the form

$$n(x) = \frac{N}{\sigma_x\sqrt{2\pi}} \exp - [(x - x_0)^2/2\sigma_x^2], \quad (1)$$

where $x = \ln(r)$, $x_0 = \ln(r_0)$, and r_0 is the modal radius in microns; N is the total number of drops per unit

volume; and σ_x is the logarithmic width of the distribution. An example of the distribution is shown in Fig. 1. The kth moment of this distribution is

$$\langle r^k \rangle = N^{-1} \int r^k n(x) dx = N^{-1} \int r^k n(r) dr$$
$$= r_0^k \exp(k^2 \sigma_x^2 / 2). \quad (2)$$

b. Droplet parameters

Various properties of the drizzle at some height z can be computed from the moments of the distribution. For example, the liquid water content q_l is given by

$$q_l = (4\pi/3)\rho_w N \langle r^3 \rangle = (4\pi/3)\rho_w N r_0^3 \exp(9\sigma_x^2/2), \quad (3)$$

where ρ_w is the density of water. The reflectivity factor Z is given by

$$Z = 2^6 N \langle r^6 \rangle = 2^6 N r_0^6 \exp(18\sigma_x^2). \quad (4)$$

The vertical flux of liquid water associated with the drizzle falling in still air is given by

$$F_q = -(4\pi/3)\rho_w \int V_f(r) r^3 n(r) dr, \quad (5)$$

where $V_f(r)$ is the radius-dependent mean fall velocity of the droplets. We use the sign convention that V_f is positive for an object that is falling and the Doppler velocity is positive for motion toward the radar.

c. Radar backscatter spectrum

The radar scattering properties of the droplet distributions are expressed in terms of the radar reflectivity (backscattering cross section per unit volume) η and the incremental scattering contribution of each size droplet as estimated by the standard Rayleigh approximation (Battan 1973):

$$\frac{\partial \eta}{\partial r} = 4\pi(2\pi/\lambda)^4 |K|^2 r^6 n(r), \quad (6)$$

where $|K|^2 = 0.93$ is the refractive index factor for liquid water and λ is the radar wavelength. Thus, η is the integral of (6) over all droplets:

$$\eta = \int \frac{\partial \eta}{\partial r} dr = \pi^5 \lambda^{-4} |K|^2 Z. \quad (7)$$

The reflectivity factor dBZ is given by

$$\mathrm{dBZ} = 10 \log(Z) + 180, \quad (8)$$

where the factor 180 results because Z is expressed in units of cubic meters (m^3), while the dBZ notation assumes conventional units ($mm^6\ m^{-3}$).

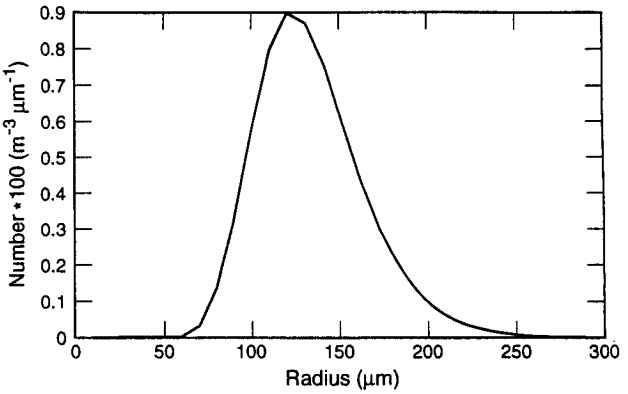

FIG. 1. Sample distribution function of drizzle droplets. The modal radius is 120 μm, and the standard deviation is 0.35 μm.

d. Doppler spectrum

The fundamental measurement of a Doppler radar is the Doppler spectrum. The Doppler spectrum $\partial\eta/\partial V$ is defined as the backscatter intensity detected between Doppler velocities $V - dV/2$ and $V + dV/2$ or, alternatively, the reflectivity-weighted velocity distribution. The Doppler spectrum is directly related to the backscatter distribution defined in (6) through the fall velocity dependence on radius

$$\frac{\partial \eta}{\partial V} = \frac{\partial \eta}{\partial r}\frac{\partial r}{\partial V_f} = 4\pi(2\pi/\lambda)^4 |K|^2 r^6 \frac{\partial r}{\partial V_f} n(r). \quad (9)$$

The kth velocity moment is then expressed as

$$\langle V^k \rangle_D = \eta^{-1} \int V^k \frac{\partial \eta}{\partial V} dV = \eta^{-1} \int [V_f(r)]^k \frac{\partial \eta}{\partial r} dr$$
$$= \langle r^6 [V_f(r)]^k \rangle / \langle r^6 \rangle, \quad (10)$$

where $\langle\ \rangle_D$ denotes a velocity moment taken from the Doppler spectrum.

3. Application to cloud and drizzle

a. Drizzle velocity moments

Once we specify $V_f(r)$, we can use (10) to determine the characteristic parameters for (3), (4), and (5). We restrict our definition of drizzle to the range of droplet sizes characterized by the linear droplet-fall-velocity relationship (Gossard et al. 1990):

$$r = aV_f + b, \quad (11)$$

where $a = 1.2 \times 10^{-4}$ s and $b = 1.0 \times 10^{-5}$ m. This approximation is reasonable for 45 μm $< r <$ 400 μm and for 0.3 m s^{-1} $< V_f <$ 3.0 m s^{-1}. Of course, more general forms of (11) can be specified, but we do not feel that the much messier mathematics is necessary for our purposes. We prefer to consider particles smaller than 45 μm as "cloud droplets" and those larger than 400 μm as "raindrops."

TABLE 1. Parameters used to discriminate between cloud and drizzle returns.

Parameter	Cloud	Drizzle
σ_x	0.35	0.35
q_l (g m^{-3})	0.38	0.02
N (cm^{-3})	100	—
r_0 (μm)	—	60
dBZ*	−18	−5
$\langle V_D\rangle$* (m s^{-1})	0.066	0.97

* Values of these parameters result from the values of the other four parameters.

Using (10) and (11) it is easy to compute the mean Doppler velocity:

$$a\langle V\rangle_D + b = r_0 \exp(13\sigma_x^2/2). \quad (12)$$

The Doppler width σ_v is given by

$$\sigma_v^2 = \langle V^2\rangle_D - (\langle V\rangle_D)^2$$
$$= (r_0/a)^2 \exp(13\sigma_x^2)[\exp(\sigma_x^2) - 1]. \quad (13)$$

There are two components to σ_v^2. There is spectral broadening in the individual pulse volume, which yields the velocity variance in the pulse volume, and there is the variance of the mean vertical velocity due to the pulse volume to pulse volume variation. Intuitively, we can see this if we had a pulse volume that was small enough to see only one-droplet fall velocity. Then the variance in the Doppler velocity would consist only of the pulse volume to pulse volume variation. However, if the pulse volume were so large that it contained all of the drizzle droplets, then all of the variance in the vertical velocity would be in the second moment of the Doppler spectrum, and the pulse volume to pulse volume variation would be zero. Our measurements, of course, are in between, which is why we include both contributions. Combining (12) and (13), we can solve for the logarithmic width

$$\sigma_x = (\ln[1 + \sigma_v^2/(\langle V\rangle_D + b/a)^2])^{1/2} \approx \sigma_v/\langle V\rangle_D. \quad (14)$$

Using (3) and (4), we can express Z in terms of the drizzle liquid water content; using (12) to eliminate the modal radius yields

$$Z \approx \frac{48}{\pi}(q_l/\rho_w)(a\langle V\rangle_D)^3 \exp(-6\sigma_x^2). \quad (15)$$

This gives us a relation for the drizzle liquid water content expressed in units of grams per cubic meter:

$$q_l = (a\langle V\rangle_D)^{-3} 10^{(\mathrm{dBZ} - 132 + 26\sigma_x^2)/10}, \quad (16)$$

where the factor 132 is $[180 + 10\log(48/(\pi\rho_w)]$ with the density of water 1×10^6 g m^{-3}, and the factor 26 is $10[6\log(e)]$. Finally, the drizzle moisture flux is

$$F_q = -q_l\left[\left(\langle V\rangle_D + \frac{b}{a}\right)\exp(-3\sigma_x^2) - \frac{b}{a}\right]. \quad (17)$$

Note that b/a is about 0.08 m s^{-1}.

b. Cloud versus drizzle droplets

Our intent is to diagnose drizzle and cloud properties by processing the Doppler radar data. Because we expect clouds and drizzle to coexist in a significant portion of the vertical scale (i.e., within the cloud), we must consider the ability of the radar to discriminate between cloud and drizzle returns. To do this, we return to the Doppler spectrum expressed by (9). However, we now consider the total droplet number density to be the sum of a cloud mode n_c and a drizzle mode n_d. The individual modes are described by the lognormal distribution but characterized by a different set of parameters. Following White et al. (1991), we chose the parameters as in Table 1. The values of dBZ and $\langle V\rangle_D$ result from the specifications of the other parameters in the table. The fall velocity approximation of (11) is not valid for the cloud droplets, so we use the more general form of Gossard et al. (1990) to compute $\partial r/\partial V_f$ for use in (9). The resulting Doppler spectrum is shown in Fig. 2. The cloud mode is 13 dB weaker than the drizzle mode and is restricted to the Doppler velocity bins near zero. These results suggest that we can discriminate against clouds by setting an analysis threshold based on dBZ or $\langle V\rangle_D$.

If we process the radar data assuming that the mean Doppler velocity is due solely to the drizzle, then we introduce an error because the measured Doppler is biased low by the scattering from the clouds (which have near-zero fall velocity). For the parameters in Table 1, the total mean Doppler velocity (the first moment integrated over both cloud and drizzle distributions) is 0.91 m s^{-1} or about 0.07 m s^{-1} less than the drizzle mode. A bit of simple algebra shows that if the scat-

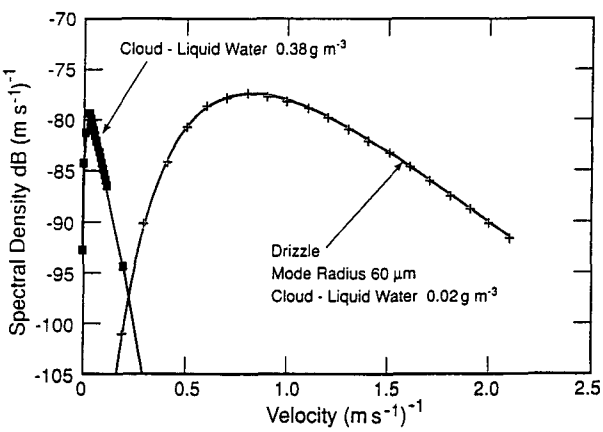

FIG. 2. Simulated Doppler spectra for cloud and drizzle versus velocity.

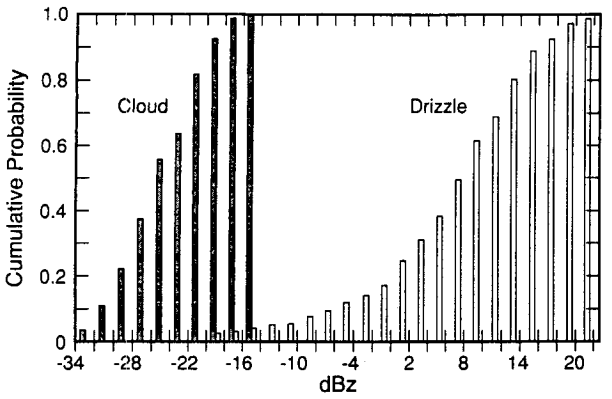

FIG. 3. Measured distribution of reflectivity for typical cloud (shaded bars) and drizzle (open bars) cases during ASTEX. Each set of measurements was made for a 23-min interval, sampled every 3 s for a total of 460 samples.

tering is dominated by the drizzle, then the fractional error in the mean velocity is approximately given by the ratio of the cloud to the drizzle scattering coefficients (in decibels, the difference in the dBZ). From (16) and (17) we can see that the derived values for the drizzle flux scale as $\langle V\rangle_D^{-2}$, so the cloud scattering bias causes us to overestimate the flux (by about 18% in this case). This suggests that in the presence of clouds with liquid water content greater than 0.4 g m^{-3} our flux estimates become unreliable for scattering intensities less than −5 dBZ.

To see how much the cloud and drizzle overlap, we computed the cumulative distribution function of measured reflectivity for typical cloud and drizzle cases from ASTEX (shown in Fig. 3). This plot shows that the reflectivity fields of the cloud and drizzle have very little overlap.

c. *Cloud properties*

In clouds, the motion of the cloud droplets is small relative to the mean air motion and the turbulent motion, so we cannot use the same method for determining the cloud liquid water as we did in the drizzle case. However, it has been noted (Davidson et al. 1984) that in stratus cloud measurements the number of droplets per unit volume is almost constant with height (see Slingo et al. 1982a; Slingo et al. 1982b; Nicholls 1987). The logarithmic spread is also constant with height and has a typical value of about 0.35. For a given value of N, we can determine the profiles of liquid water within the cloud from the measured reflectivity using (3) and (4):

$$q_l = 0.30\rho_w Z^{1/2} N^{1/2}. \qquad (18)$$

Furthermore, by using the integrated liquid water from the radiometer, we can adjust N to fit the radiometer measurement of total integrated liquid water. Having obtained values of the three basic droplet distribution parameters, we can compute any related droplet microphysical parameters.

4. Descriptions of the radar, radiometer, experiment, and data processing

The radar used for this study was the National Oceanic and Atmospheric Administration (NOAA) Environmental Technology Laboratory (ETL) K_α-band radar. This radar is sensitive enough to measure clouds and was originally discussed by Pasqualucci et al. (1983). The characteristics of the radar are given in Table 2. The radar site was on the northern edge of the island, near the commercial runway. It was positioned 100 m from the edge of a 100-m cliff, which was as close to the edge as possible. The ground clutter for the vertical mode was caused by a gradual rise over 2 km to two small peaks with an elevation of about 1.5 km. This ground clutter affected only the first 200 m of vertical measurements.

The Doppler processing was the conventional pulse-pair technique to obtain real-time velocity measurements. The spread of the Doppler spectrum was also estimated by this technique. For drizzle, for which the signal-to-noise ratio is high, the spectral width measurements are reliable.

The microwave radiometer employed at ASTEX is a three-frequency system for the simultaneous measurement of atmospheric water vapor and liquid water in clouds; details of the system were given by Hogg et al. (1983). The system is completely passive, using the natural emission of microwave energy by water vapor and liquid water. Measured values are total liquid water and water vapor integrated along the atmospheric path being observed by the radiometer antenna beam. The system contains three independent channels: the first operates at a wavelength of 1.46 cm (20.6 GHz), which is sensitive primarily to water vapor; the second operates at a wavelength of 0.95 cm (31.65 GHz), which is sensitive primarily to liquid water; and the third operates at a wavelength of 0.33 cm (90 GHz), which is sensitive to both vapor and liquid. However, the third channel is approximately six times more sensitive to

TABLE 2. Characteristics of the K_α-band radar.

Characteristic	Values
Antenna size	1.2 m
Beamwidth	0.5°
Maximum sidelobe	−30 dB relative to main
Wavelength	8.66 mm
Peak power	100 kW
Pulse length	0.25 μs
Pulse repetition frequency	Variable (2000/s typical)
Scanning	Full PPI, sector, over-top
Noise power (linear receiver)	−98 dBm

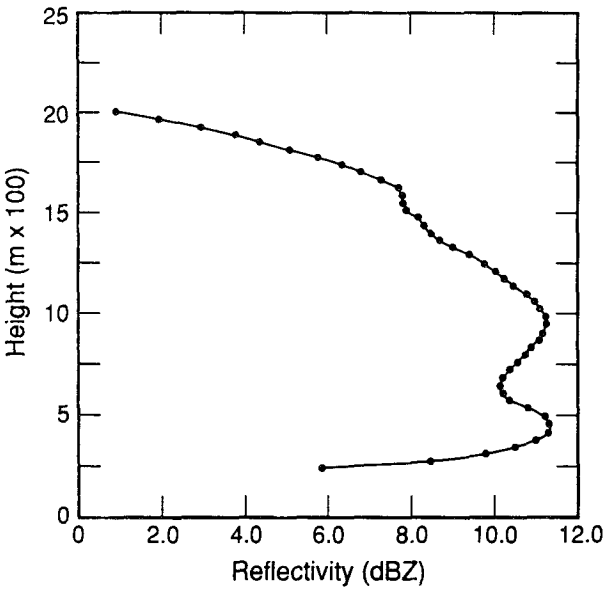

FIG. 4. Average reflectivity from the K_α-band radar for the drizzle case, 0600–0625 UTC 6 June 1992. Cloud boundaries were determined from the radar reflectivity just prior to the drizzle.

liquid water than is the second channel. The three radiometers are coupled into a common antenna system with concentric beams of equal 2.5° width. Although the antenna system is steerable in both azimuth and elevation, the antenna beams were directed only to the zenith for the measurement period.

The statistical retrieval technique was described by Hogg et al. (1983). The estimated uncertainty in the liquid measurement is 20%. System outputs were averaged over 30 s for most of the ASTEX operation.

5. Results

The first drizzle period we studied was 6 June 1992 from 0600 to 0625 UTC. We averaged our measurements over this interval in order to average out the vertical air motion that could cause significant error in our calculations, depending on the drizzle fall speed and the vertical air motion. In our case, the average Doppler velocity varied from about 1 to 3 m s^{-1}. To see if the airflow over the island was significant, we averaged the vertical velocity in cloud for about 12 min prior to the drizzle event. We calculated that when we use a low reflectivity as a threshold (<20 dBZ), the fall velocity of the cloud particles should be less than 2 cm s^{-1} and the vertical Doppler velocity is a good indication of the air motion. For this 12-min period, the Doppler velocity averaged out to be less than a few centimeters per second.

Figure 4 shows the average reflectivity profile for the time interval of the first drizzle event. Since the drizzle reflectivity will overwhelm the cloud reflectivity, we used the reflectivity just prior to the start of the drizzle to determine the cloud boundaries. During the drizzle, the cloud top rises about 200 m compared with the nondrizzle cloud just before the drizzle. The cloud base just prior to the drizzle was about 600 m. The increase in the cloud-top heights during drizzle was observed often by D. H. Lenschow (1993, personal communication) in aircraft flights in other ASTEX areas.

Note the bump in reflectivity at 500 m. Normally, one would expect the drizzle liquid water (and reflectivity) to decrease uniformly below the cloud from a maximum near cloud base as the droplets evaporate. However, the drizzle droplets are falling through a region of vertical shear (shown by the Colorado State University wind profiler measurements in Fig. 5) and a vertical cut may not adequately sample the droplets at all heights. The effects of this bump will carry through several parameters such as liquid water, liquid water flux, and number of droplets.

The modal radius is shown in Fig. 6. Near the top of the cloud, the radius varies between 20 and 40 μm, increasing gradually from 1400 m to about 160 μm at the lowest measurement height. We estimate the measurement uncertainty of the radius to be about 10% (see the appendix). The second drizzle parameter, the standard deviation (Fig. 7), shows a decrease from about 0.65 at the cloud top to a minimum of 0.36 at 300 m. The error in this estimate should be about 7%. Finally, the third parameter, the number of drops (Fig. 8) shows considerable variability near cloud top from 20 to 10 000 l^{-L}, decreasing to about 0.2 l^{-L} at 250 m. Most rapid variations with height occur from about 1400 m to cloud top. The vertical velocity measurements show strong upward motion persisting for a few minutes in this range. Our averaging time may have been too short to average this effect out. (Negative

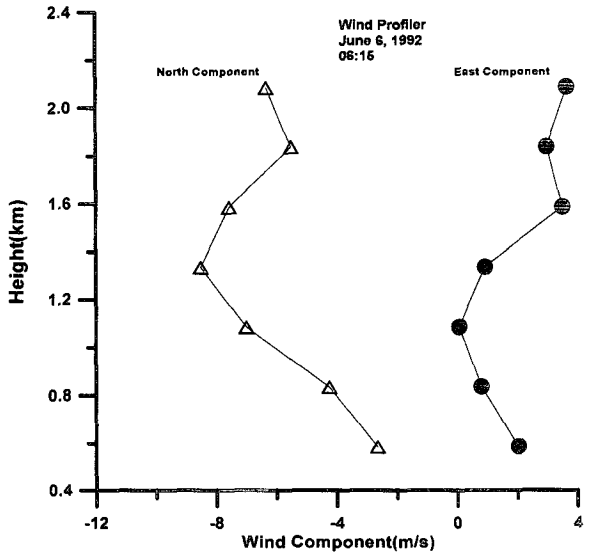

FIG. 5. Wind profiler measurements of horizontal winds.

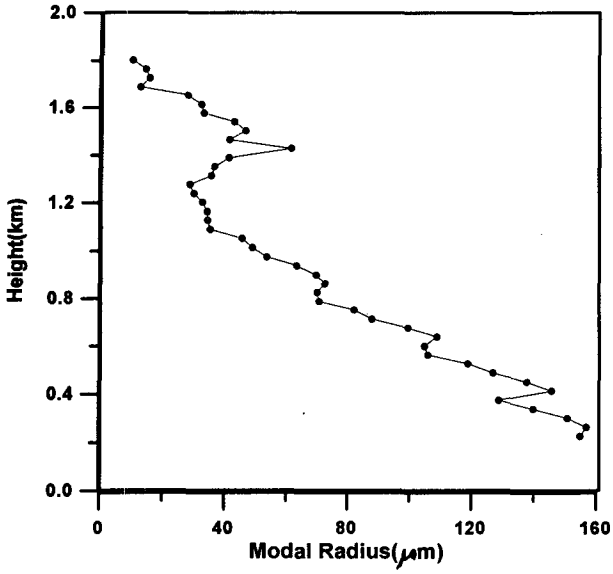

FIG. 6. Drizzle modal radius versus height, 0600–0625 UTC 6 June 1992.

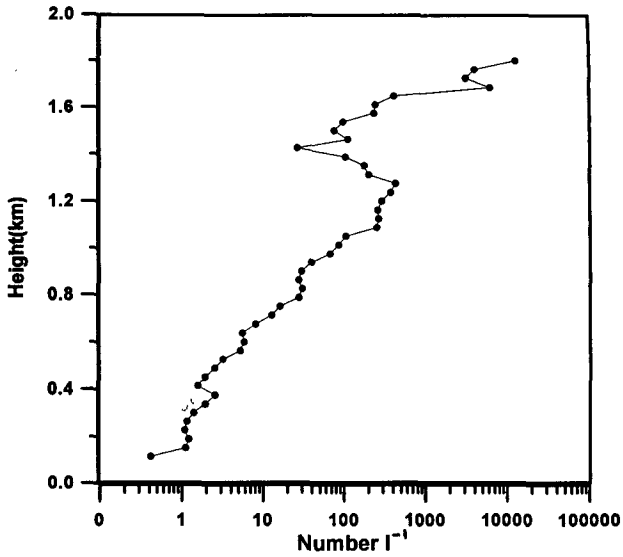

FIG. 8. Number of drizzle drops per liter versus height, 0600–0625 UTC 6 June 1992.

Doppler velocity can be caused only by upward air motion.) We estimate the error in this calculation to be about 36% (see the appendix).

The next parameter is the vertical profile of liquid water, which is shown in Fig. 9. There is a maximum of about 0.5 g m^{-3} at 1800 m, with large variations above and below. Below 1400 m, the liquid water decreases to 0.03 at 250 m. For this measurement, we estimate the liquid water random measurement error on the order of 11% and 46% if we include a bias in the reflectivity (see the appendix). An additional quantity of interest is the mean vertical liquid water flux, which is shown in Fig. 10. By smoothing this flux and computing the divergence, we can estimate the effective rate of cooling and heating due to this flux (Fig. 11). This figure shows that in the lower part of the cloud and below the cloud (cloud base ~500–600 m) the liquid water flux divergence cools the air by as much as 4.0°C h^{-1} and that in the upper part of the cloud there is an effective warming with a maximum rate of

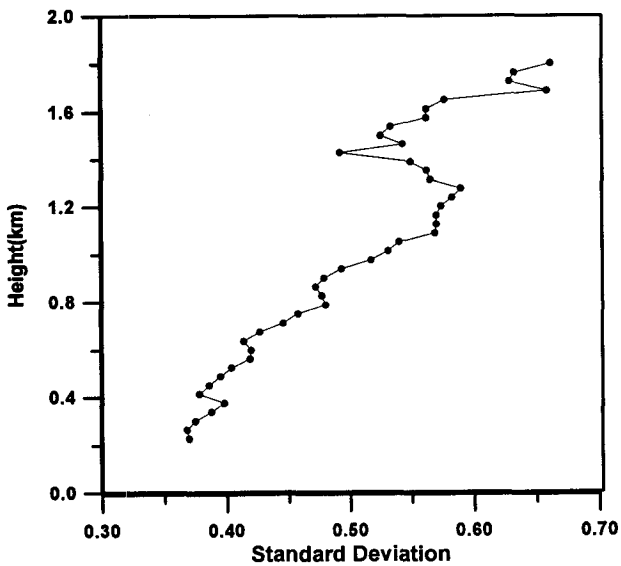

FIG. 7. Drizzle droplet lognormal standard deviation versus height, 0600–0625 UTC 6 June 1992.

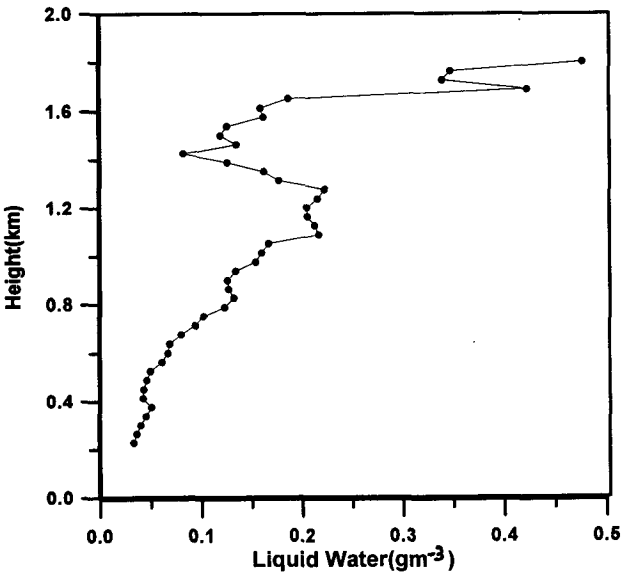

FIG. 9. Drizzle liquid water versus height, 0600–0625 UTC 6 June 1992.

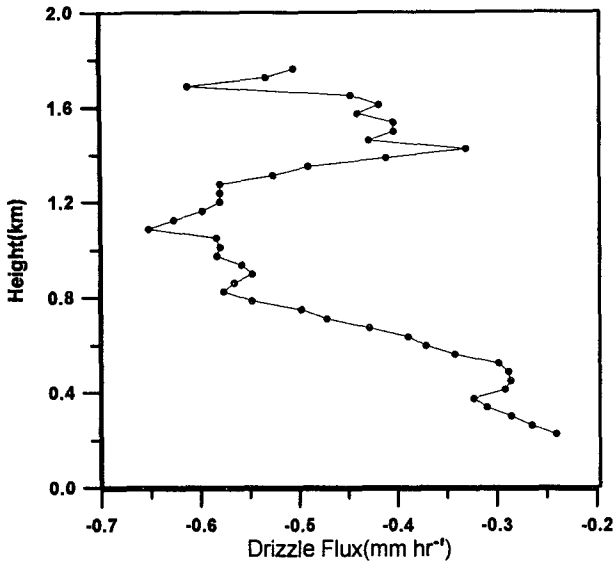

FIG. 10. Mean vertical flux of drizzle liquid water versus height, 0600–0625 UTC 6 June 1992.

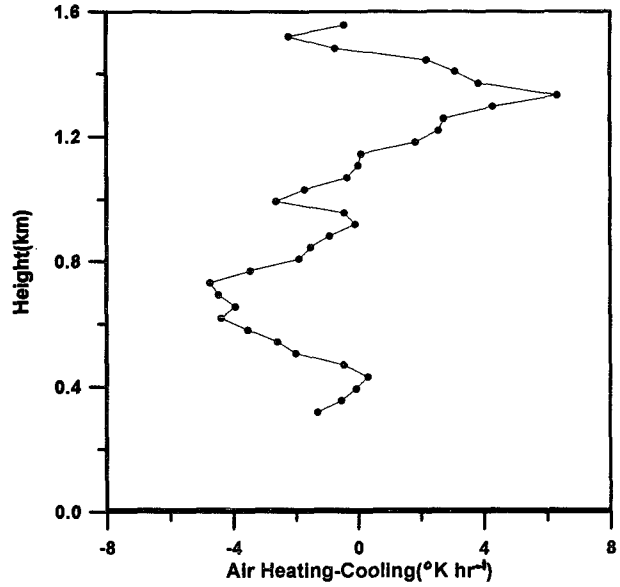

FIG. 11. Air heating and cooling from the mean liquid water flux divergence in drizzle versus height, 0600–0625 UTC 6 June 1992.

about 6°C h^{-1} if the cloud is in steady state. Much of the variation with height is due to the effect of random errors in the derivative calculations. In addition, in the liquid water, liquid water flux, and heating–cooling calculation there is a change in the behavior below about 700 m. This is caused by an increase in the drizzle reflectivity (Fig. 4). Below the cloud, this effective cooling site is due to evaporation and is a real cooling, as described by the profile. Within the cloud, the divergence of the drizzle flux is primarily caused by collisional accretion of the cloud water onto the falling drizzle drops, so no real exchange of heat is directly involved. However, to maintain equilibrium, the cloud must replace this lost liquid water by condensing vapor and releasing an equivalent latent heat, although this heat is not necessarily realized in the same location as the drizzle removal of cloud liquid water. Thus, even in dynamic equilibrium, the condensational heating may not have the same profile as the effective heating profile computed from the drizzle. (The vertical integrals must be the same.)

The observed steady increase of drizzle flux, water content, and characteristic width and radius from cloud top downward within the cloud are consistent with the growth of the drizzle mode by collisional and turbulent coalescence with cloud droplets, as described by Nicholls (1987). These processes cease to be effective just above the cloud bottom where the cloud liquid water content is approaching zero. Below the cloud, evaporation removes the smaller droplets very quickly, causing the drizzle distribution to narrow (the width decreases) and the modal radius to increase. Obviously, the downward drizzle flux and the drizzle liquid water content are also decreased by evaporation. Except for the anomalous maximum in reflectivity observed well below cloud base, this limited case example is consistent with the expected physical processes.

As an example of the cloud property technique, we used data taken simultaneously with the radiometer and the radar during a second period we studied. It started at 0000 UTC and ended at 1800 UTC 17 June 1992. We used the radiometer-derived liquid water and the

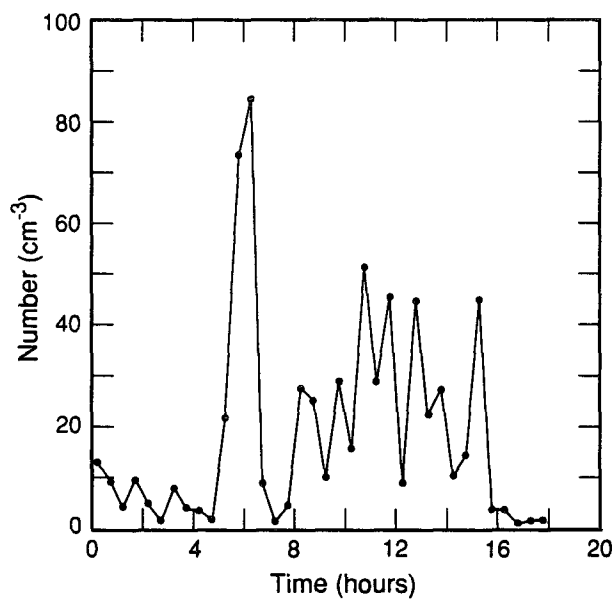

FIG. 12. Number of cloud drops per cubic centimeter versus time, 17 June 1992.

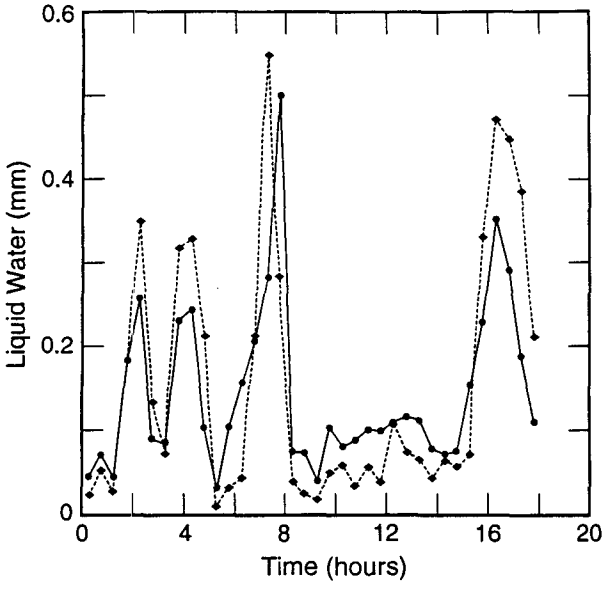

FIG. 13. Radar-derived integrated liquid water assuming 25 droplets/cm^{-3} and radiometer total liquid water measurement (solid curve) versus time for 17 June 1992.

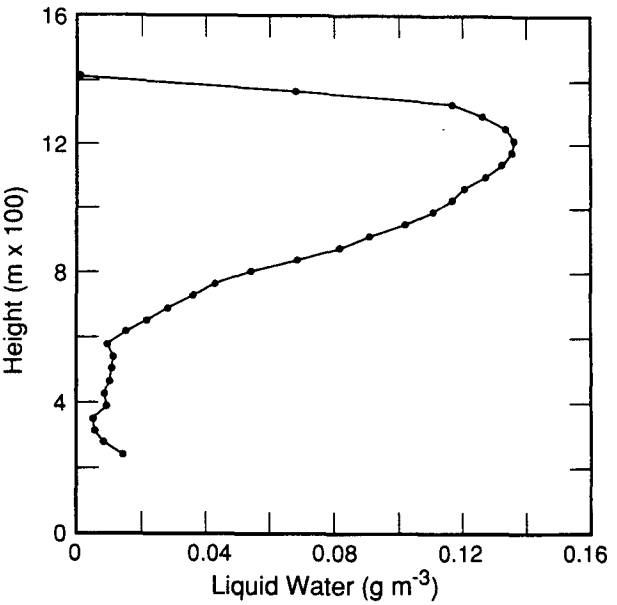

FIG. 14. Liquid cloud water profile, 1400–1423 UTC 17 June 1992.

radar reflectivity to estimate the droplet concentration as a function of time. The radar and radiometer data were averaged over a 23-min period. Figure 12 shows a time series of deduced values N for an 18-h period. During some of this time, there was drizzle, which invalidates our calculation assumptions for cloud properties. In addition, the zero line accuracy of the radiometer of 0.1 mm seriously limits the accuracy for the determination of N for thin clouds. The actual radiometer-derived integrated liquid water time series is shown in Fig. 13, along with the radar-derived liquid water assuming a droplet concentration of 25 cm^{-3}. The very large spikes coincide with drizzle times.

Once we determined the cloud droplet concentration, we could determine the liquid water profile and, with the Doppler information, the mean liquid water flux. Figure 14 is a liquid water profile measured from 1400 to 1423 UTC 17 June 1992. The liquid water maximum is 0.14 g m^{-3} at about 1200 m. The corresponding modal radius is shown in Fig. 15 with a maximum value of 12 μm at 1200 m, decreasing in size at lower heights. Again, these measured profiles of liquid water content and modal radius are quite consistent with those previously observed in stratocumulus clouds. However, the observed liquid water content is about one-tenth the adiabatic value.

The liquid water flux is displayed in Fig. 16. Here the liquid water flux is computed from the droplet fall speed. The observed magnitude of the flux is a maximum at 1200 m and negative in value. The divergence of this flux is positive above 1200 m and negative below. This is equivalent to cooling in the lower levels of the cloud and warming in the upper part of the cloud. For equilibrium to be maintained, the mean cloud liquid flux would have to be counterbalanced by the turbulent fluxes of liquid water and turbulent and mean advection of water vapor. Of course, to the extent that the mean loss is balanced by turbulent transport of liquid water, there will be no thermodynamic effects.

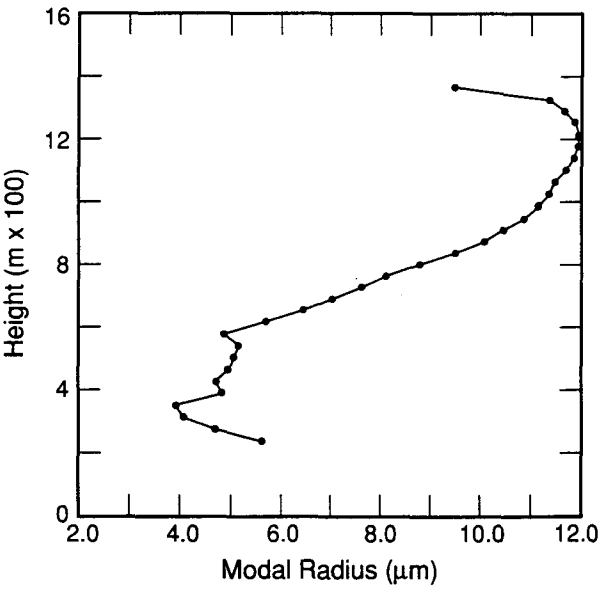

FIG. 15. Cloud modal radius profile, 1400–1423 UTC 17 June 1992.

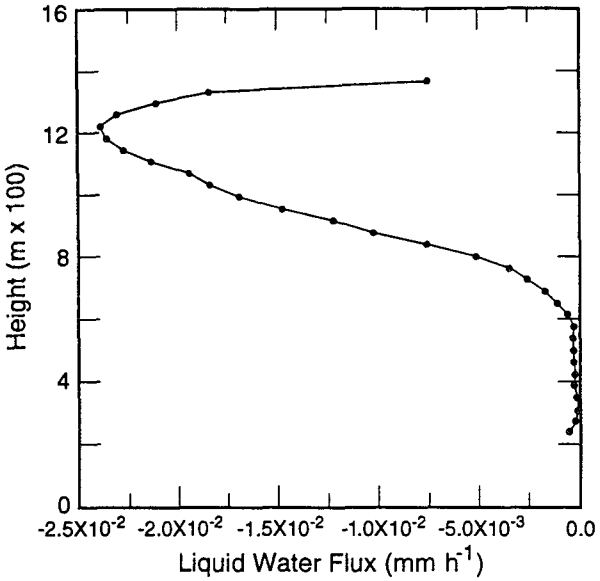

FIG. 16. Cloud mean liquid water flux, 1400–1423 UTC 17 June 1992.

6. Conclusions

We have shown a technique that uses a K_a-band Doppler radar and a simple drizzle model to determine various parameters of drizzle in stratocumulus clouds. By using the zeroth, first, and second moments of the Doppler velocity, we have determined the number, size distribution, liquid water, mean liquid water flux, and mean rate of condensation and evaporation by the divergence of this mean liquid water flux.

To minimize the effects of the turbulent vertical velocity on estimates of mean fall speeds, we averaged over a 23-min interval. If the drizzle periods are longer, a longer average would be in order. Even with this long average, there was a strong updraft above 1500 m that probably biased the velocity measurements and contributed to errors in our parameters. Horizontal inhomogeneity in the drizzle can also confuse the interpretation from a simple one-dimensional point of view. To minimize the effects of updrafts and inhomogeneity, averages of many events are necessary. This will be our next step in the ASTEX analysis.

In another technique that combines radar reflectivity and microwave radiometer integrated cloud liquid water data, we have shown how to estimate profiles of liquid water and liquid water flux in stratus clouds using a simple lognormal model of cloud drops and an assumption that the droplet concentration in nonprecipitating clouds is constant with height. This assumption is based on many observations of stratus clouds.

These results demonstrate that there is a potential for surface-based remote sensors to do long-term monitoring of cloud and drizzle droplet parameters. This has considerable promise as a tool for research on cloud microphysical processes associated with precipitation formation, evaporation, and dynamical implications and for cloud–radiation interactions (e.g., Chertock et al. 1993). Because the radar measures all parts of the profile simultaneously, the data are appropriately sampled for taking the vertical derivative. Thus, it offers an excellent complement to the horizontal averaging that is the strength of aircraft.

Acknowledgments. This work was partially supported by the NOAA Climate and Global Change Program and the Department of Energy Atmospheric Radiation Measurement Program (ARM). The authors wish to thank Bruce Bartram, Janet Gibson, Bob Kropfli, Duane Hazen, and Anthony Francavilla of the Environmental Technology Laboratory, and Wayne Schubert of Colorado State University, for their assistance during this project. They would also like to thank Xiquan Dong at Penn State University for comments on the manuscript.

APPENDIX

Drizzle Parameter Error Estimates

There are two obvious sources of error in the method we have developed: 1) errors induced by errors in the measured parameters, and 2) errors caused by approximating the true droplet spectrum with a lognormal. The first point we can evaluate straightforwardly by applying standard error analysis to our expressions for the various derived quantities (see below). However, we can state that Gossard (1994) has found his method of deducing droplet moments from Doppler spectra to be insensitive to the choice of Gamma versus lognormal distribution.

Although we cannot estimate the errors directly in all of the drizzle terms, we can make reasonable estimates of those errors. In the estimates of the drizzle parameters, there are the errors in the first three Doppler moments. The zeroth moment or backscattered power error estimate will be smaller for the higher signal-to-noise ratios such as found in drizzle. Since we are averaging the power estimates over many measurements, the random error in the estimate will be reduced by $1/N^{1/2}$, where N is the number of independent samples. For our case, this will reduce the random error by about $1/20$. In the range of reflectivities that we use, the random error in backscattered power is about 0.1 dBZ per estimate; thus, the total random error is about 0.005 dBZ. We estimate the bias error to be less than 2.0 dBZ.

The error in the mean Doppler velocity is estimated using a method given by Dennenberg (1971). With this particular radar, the error should be less than 0.01 m s^{-1}. Probably a larger error will be due to the assumption of zero-mean vertical air motion. For example, if the updrafts and the downdrafts are of sufficient duration, they may not average to a sufficiently small value relative to the droplet fall speed. However, ac-

cording to D. Lenschow (1992, personal communication), aircraft measurements in stratus in the ASTEX area were several meters per second and a few hundred meters in extent. Since our averaging is equivalent to a several kilometer sample, this should not be a significant effect. We will use a number on the order of 0.1 m s^{-1} as an error estimate. Another potential error in the mean Doppler fall velocity is the mean vertical air motion induced by the airflow over the island. To estimate this error, we can look at the mean vertical motion just prior to the drizzle and just afterward as an estimate. In the 6 June 1992 event, we have good enough reflectivity values in the cloud to measure mean Doppler velocity values that are on the order of 0.2 m s^{-1}.

The third error in our observations would be in the estimates of the second moments of the vertical velocity. Part of the second moment comes from the sample variance of the first moment; the other will be from the estimate of the variance of the Doppler spectra. The variance error due to the errors in the first moment estimate will be reduced by $1/N^{1/2}$, which in our case will be roughly $1/20$. For an uncertainty as small as we have in the first moment estimate, this error will be insignificant. One contribution to both variances is turbulent air motion. We examined the in-cloud turbulence just prior to the drizzle and found it to be on the order of 0.1 m^2 s^{-2} for the variance components. This is probably the largest error, since it combines turbulence and measurement errors in a low signal-to-noise case. In drizzle, the signal-to-noise ratio is much higher and the measurement errors are smaller.

The errors in the spread can be written as

$$\frac{\epsilon_{\sigma_x}}{\sigma_x} = \left[\left(\frac{\epsilon_{V_D}}{V_D}\right)^2 + \left(\frac{\epsilon_{\sigma_V}}{\sigma_V}\right)^2\right]^{1/2},$$

where ϵ denotes the errors associated with the Doppler velocity V_D and the second moment σ_V. If we use a 5% error in each term, then the error in the spread will be about 7%.

To get the errors in the drizzle liquid water concentration, we note that the liquid water can be written as

$$q_l = V(V_D)S(\sigma_x)D\,(\mathrm{dBZ}),$$

where

$$V = \frac{1}{aV_D^3},$$

$$S = 10^{2.6\sigma_x^2},$$

and

$$D = 10^{\mathrm{dBZ}/10}.$$

The relative error in the liquid water can be written as

$$\frac{\epsilon_{q_l}}{q_l} = \left[\left(\frac{\epsilon_V}{V}\right)^2 + \left(\frac{\epsilon_S}{S}\right)^2 + \left(\frac{\epsilon_D}{D}\right)^2\right]^{1/2},$$

where

$$\epsilon_S = 12 \times 10^{2.6\sigma_x^2}\sigma_x\epsilon_{\sigma_x},$$

$$\epsilon_D = 0.23 \times 10^{\mathrm{dBZ}/10}\epsilon_{\mathrm{dBZ}},$$

and

$$e_V = -3\,\frac{\epsilon_{V_D}}{aV_D^4},$$

and ϵ_{dBZ} is the radar reflectivity measurement error. If we assume that the random error in power is 0.1 dBZ, the velocity 5%, and the second moment 5%, then for a $\sigma_x = 0.35$ the random error in the drizzle liquid water concentration will be about 11%. The absolute liquid water error will be about 46% with a 2-dBZ error in reflectivity.

A similar analysis can be done for the modal radius. In this case, the radius is dependent only on the first and second moments of the Doppler velocity. With the values used, this gives an absolute error of about 10% in the modal radius calculation.

REFERENCES

Albrecht, B. A., 1989: Aerosols, cloud microphysics, and fractional cloudiness. *Science,* **245,** 1227–1230.

——, 1993: The effects of precipitation on the thermodynamic structure of trade-wind boundary layers. *J. Geophys. Res.,* **98,** 7327–7337.

——, D. A. Randall, and S. Nicholls, 1988: Observations of marine stratocumulus clouds during FIRE. *Bull. Amer. Meteor. Soc.,* **69,** 618–626.

Atlas, D., D. Short, and D. Rosenfeld, 1989: Climatologically tuned reflectivity rain-rate relations. *Proc. 24th Conf. on Radar Meteorology,* Tallahassee, FL, Amer. Meteor. Soc., 666–671.

Baker, M. B., and R. J. Charlson, 1990: Bistability of CCN concentrations and thermodynamics in the cloud-topped boundary layer. *Nature,* **345,** 142–145.

Battan, L. J., 1973: *Radar Observations of the Atmosphere.* University of Chicago Press, 324 pp.

Bechtold, P., C. Fravalo, and J. P. Pinty, 1992: A model of marine boundary-layer cloudiness for mesoscale applications. *J. Atmos. Sci.,* **49,** 1723–1744.

Betts, A. K., 1989: The diurnal variation of California coastal stratocumulus from two days of boundary layer soundings. *Tellus,* **42A,** 302–304.

——, and W. Ridgway, 1989: Climatic equilibrium of the atmospheric convective boundary layer over a tropical ocean. *J. Atmos. Sci.,* **46,** 2621–2641.

Borovikov, A. M., 1961: *Cloud Physics.* Gidrometeoizdat, 459 pp.

Brost, R. A., J. C. Wyngaard, and D. H. Lenschow, 1982: Marine stratocumulus layers. Part II: Turbulence budgets. *J. Atmos. Sci.,* **39,** 818–836.

Chertock, B., C. W. Fairall, and A. B. White, 1993: Surface-based measurements and satellite retrievals of broken cloud properties in the equatorial Pacific Ocean. *J. Geophys. Res.,* **98,** 18 489–18 500.

Davidson, K. L., C. W. Fairall, P. Jones Boyle, and G. E. Schacher, 1984: Verification of an atmospheric mixed-layer model for a coastal region. *J. Climate Appl. Meteor.,* **23,** 617–636.

Dennenberg, J. N., 1971: The estimates of spectral moments. Tech. Rep. No. 23, Laboratory for Atmospheric Probing, University of Chicago and Illinois Institute of Technology, 71 pp.

Duynkerke, P. G., and A. G. M. Driedonks, 1987: A model for the turbulent structure of the stratocumulus-topped atmospheric boundary layer. *J. Atmos. Sci.,* **44,** 43–64.

Gossard, E. E., 1994: Measurement of cloud droplet size spectra by Doppler radar. *J. Atmos. Oceanic Technol.*, **11,** 712–726.

——, R. G. Strauch, and R. R. Rogers, 1990: Evolution of drop-size distributions in liquid precipitation observed by ground-based Doppler radar. *J. Atmos. Oceanic Technol.*, **7,** 815–828.

Hogg, D. C., F. O. Guiraud, J. B. Snider, M. T. Decker, and E. R. Westwater, 1983: A steerable dual-channel microwave radiometer for measurement of water vapor and liquid in the atmosphere. *J. Appl. Meteor.*, **22,** 789–906.

Kropfli, R. A., B. W. Bartram, and S. Y. Matrosov, 1990: The upgraded WPL dual-polarization 8-mm wavelength Doppler radar for microphysical and climate research. *1990 Conf. on Cloud Physics,* San Francisco, CA, Amer. Meteor. Soc., 341–345.

Levin, L. M., 1961: *Studies of Physics of Large Aerosols.* USSR Academy of Sciences, 267 pp.

Marshall, J. S., and W. M. K. Palmer, 1948: The distribution of raindrops with size. *J. Meteor.*, **5,** 165–166.

Nicholls, S., 1987: A model of drizzle growth in warm, turbulent, stratiform clouds. *Quart. J. Roy. Meteor. Soc.*, **113,** 1141–1170.

——, and J. Leighton, 1986: An observational study of the structure of stratiform cloud sheets. Part I: Structure. *Quart. J. Roy. Meteor. Soc.*, **112,** 431–460.

Pasqualucci, F. B., B. W. Bartram, R. A. Kropfli, and W. R. Moninger, 1983: A millimeter-wavelength dual-polarization Doppler radar for cloud and precipitation studies. *J. Climate Appl. Meteor.*, **22,** 758–765.

Randall, D. A., 1980: Conditional instability of the first kind upside-down. *J. Atmos. Sci.*, **37,** 125–130.

——, J. A. Coakley, C. W. Fairall, R. A. Kropfli, and D. H. Lenschow, 1984: Outlook for research on subtropical marine stratiform clouds. *Bull. Amer. Meteor. Soc.*, **65,** 1290–1301.

Slingo, A. S., S. Nicholls, and J. Schnetz, 1982a: Aircraft observations of marine stratocumulus during JASIN. *Quart. J. Roy. Meteor. Soc.*, **108,** 833–856.

——, R. Brown, and C. L. Wiench, 1982b: A field study of nocturnal stratocumulus: III. High resolution radiative and microphysical observations. *Quart. J. Roy. Meteor. Soc.*, **108,** 145–166.

Telford, J. W., and P. B. Wagner, 1981: Observations of condensation growth determined by entity type mixing. *Pure Appl. Geophys.*, **119,** 934–965.

Ulbrich, C. W., 1983: Natural variations in the analytical form of the raindrop size distribution. *J. Climate Appl. Meteor.*, **22,** 1764–1775.

Wang, S., 1993: Modeling marine boundary-layer clouds with a two-layer model: A one-dimensional simulation. *J. Atmos. Sci.*, **50,** 4001–4021.

White, A. B., C. W. Fairall, and D. W. Thomson, 1991: Radar observations of humidity variability in and above the marine atmospheric boundary layer. *J. Atmos. Oceanic Technol.*, **8,** 639–658.

Willis, P. T., 1984: Functional fits to some observed drop size distributions and parameterization of rain. *J. Atmos. Sci.*, **41,** 1648–1661.

Wiscombe, W. J., R. M. Welch, and W. D. Hall, 1984: The effects of very large drops on cloud absorption. Part I: Parcel models. *J. Atmos. Sci.*, **41,** 1336–1355.